Kirill Shmulovich · Colin Graham · Bruce Yardley

Quartz, albite and diopside solubilities in H$_2$O–NaCl and H$_2$O–CO$_2$fluids at 0.5–0.9 GPa

Abstract The solubility of quartz and incongruent dissolution ('apparent solubility') of albite and diopside in H$_2$O–NaCl and H$_2$O–CO$_2$ fluids have been determined at pressures up to 0.9 GPa (9 kbar) and temperatures of 500–900 °C. Solubilities of quartz and albite decrease with increasing salt concentration [X(NaCl)](salt-out effect), whereas the solubility of diopside increases with increasing X(NaCl)(salt-in effect). Quartz solubilities in the systems H$_2$O–NaCl and H$_2$O–CO$_2$ are very similar and are proportional to X(H$_2$O)^2. Quartz solubility in NaCl-rich brines does not change with pressure under the P–T conditions of our experiments. At 0.9 GPa and 800 °C, albite solubility in pure water is higher (∼100 g/kg H$_2$O) than that of quartz (∼74 g/kg H$_2$O), but at NaCl concentrations >6 mol% these solubilities are very similar. Albite dissolution is slightly incongruent; formation and composition of secondary and quench phases (paragonite, Na-margarite, amorphous quench spheres) indicate that the solution is enriched in SiO$_2$ and Na$_2$SiO$_3$. As fluid composition changes from H$_2$O towards more CO$_2$-rich fluids or NaCl-rich brines, the solubilities of albite and quartz decrease by about one order of magnitude, but are still measurable at X(H$_2$O) < 0.5. A thermodynamic analysis of new quartz solubility data for H$_2$O–CO$_2$ fluids at 0.9 GPa indicates that complexing is dominated by SiO$_2$.4H$_2$O for water-rich fluids, but for X(H$_2$O) < 0.7 the mean solvation number decreases to ≤ 3. This speciation is similar to that reported previously for lower pressures, and is in agreement with recent high P–T spectroscopic data for the system H$_2$O–SiO$_2$. For dissolution of quartz in both H$_2$O–CO$_2$ and H$_2$O–NaCl fluids, the molecular proportions of silica to water are almost the same at any X(H$_2$O). Assuming similar non-ideal water-salt interactions irrespective of whether the water is in the fluid or is complexed with silica, then the speciation of silica appears to be similar in both H$_2$O–CO$_2$ and H$_2$O–NaCl fluids under the experimental conditions. We conclude that the speciation of silica in both H$_2$O–CO$_2$ and H$_2$O–NaCl fluids at 0.9 GPa and 800 °C is comparable, is dominated by Si(OH)$_4$·2H$_2$O and/or hydrated species with lower hydration numbers, and is also comparable to that proposed for lower P–T conditions.

K. Shmulovich · C. Graham (✉)
Department of Geology and Geophysics,
University of Edinburgh, West Mains Road,
Edinburgh EH9 3JW, UK
E-mail: colin.graham@glg.ed.ac.uk

K. Shmulovich
Institute of Experimental Mineralogy,
Russian Academy of Sciences, 142432 Chernogolovka,
Moscow District, Russia

B. Yardley
School of Earth Sciences, University of Leeds,
Leeds LS2 9JT, UK

Editorial responsibility: I. Parsons

Introduction

Deep crustal fluids may contain large amounts of water, carbon dioxide, methane and chloride salts. Thus an understanding of the dissolution, transport and precipitation of silicate material and associated element redistribution in the deep crust and upper mantle requires knowledge of mineral solubilities in a range of fluid compositions at high pressures and temperatures. Because of the technical difficulties of carrying out solubility experiments at pressures corresponding to depths below the middle crust, few such data exist. Direct experimental observation of critical phenomena in the H$_2$O–albite system (Shen and Keppler 1997) and recent data for haplogranite and nepheline (Bureau and Keppler 1999) emphasise the importance of complete miscibility between silicate melts and hydrous fluids during hydrous melting of the deep crust or upper mantle, implying very high silicate solubilities. However, the concentrations of dissolved silicates in aqueous fluids under such near-critical P–T conditions, which must be very common in the Earth's crust, in subducted slabs and in

'cold' upper mantle, are essentially unconstrained, and are the principal objective of this study.

Phase equilibria in the system H_2O–CO_2–NaCl predict fluid immiscibility, with co-existence of brines and CO_2-rich fluids, to high temperatures in salt-rich systems in the deep Earth's crust (Skippen and Trommsdorff 1986; Shmulovich et al. 1995; Shmulovich and Graham 1999). Evidence for such immiscible systems in nature is found in: fluid inclusions in granulite and eclogite facies metamorphic rocks (e.g. Touret 1985, 1995); thermodynamic estimates of fugacities of volatile components (e.g. Lamb and Valley 1988); interstitial chloride salts in granulites (Markl and Bucher 1998). The concentrations of chloride salts in crustal fluids may be modified significantly by a range of crustal processes, including hydration/dehydration reactions, melting and melt crystallisation, and fluid immiscibility (Yardley and Bottrell 1988; Shmulovich and Graham 1996, 1999; Yardley 1996), with important implications for element transport.

Most solubility measurements of rock-forming minerals have been made at pressures ≤ 0.2 GPa (2 kbar; e.g. review by Walther 1986) or, more rarely, above 1.0 GPa (e.g. Ryabchikov et al. 1982). For quartz, data exist over a wide P–T interval (up to 2.0 GPa and 900 °C) in pure H_2O (Anderson and Burnham 1965; Manning 1994), and in aqueous chloride and hydroxide solutions to 0.4 GPa and 700 °C (Anderson and Burnham 1967), and (very recently) to 1.5 GPa and 900 °C (Newton and Manning 2000). Quartz solubility has also been measured in supercritical H_2O–CO_2 and H_2O–Ar fluid systems by Sommerfeld (1967), Novgorodov (1975) and Walther and Orville (1983) at pressures below 0.5 GPa, and by Newton and Manning (2000) at 1.0 GPa and 800 °C.

Data on the effects of dissolved salts on mineral solubilities in supercritical fluids are scarce. The effect of NaCl on quartz solubility in aqueous fluid was measured at 0.05–0.2 GPa and 200–600 °C by Xie and Walther (1993), who reported a change from a salt-out effect (decreasing solubility with increasing X(NaCl)) at low temperatures (e.g. T < 400 °C at 0.1 GPa) to a salt-in effect at higher temperatures (T > 300 °C at 0.05 GPa to T > 400 °C at 0.1 GPa). Until very recently there were no published data for silicate solubility in NaCl-rich fluids at pressures above 0.5 GPa. However, Newton and Manning (2000) have very recently published results of a study of quartz solubility in H_2O–NaCl fluids over an extensive P–T range (0.2–1.5 GPa and 500–900 °C). They showed a major change in solubility behaviour with increasing X(NaCl) at 0.2 GPa from salt-in at X(NaCl) < ~0.1 to salt-out at higher salt concentrations, and with increasing pressure at low X(NaCl) from salt-in at 0.2 GPa to salt-out above ~0.4 GPa. At 1 GPa, quartz solubility was found to decrease exponentially with increasing X(NaCl).

In NaCl-rich fluids at pressures above 0.5 GPa, recent experimental results demonstrate non-ideal behaviour of the fluid caused by interactions between dissociated salt and water (Aranovich and Newton 1996; Shmulovich and Graham 1996). High-grade metamorphic fluids in the deep crust may have very different properties from shallower hydrothermal fluids, remaining dissociated to high temperatures, but concentrations of components such as silica, which may form hydrated complexes, may be very much higher than at shallower levels.

In this study, we have measured solubilities of quartz and albite in H_2O–NaCl and H_2O–CO_2 fluids at 0.5 and 0.9 GPa. We compare our results with solubilities of quartz in H_2O–NaCl (Manning 1994; Newton and Manning 2000), and of diopside in salt solutions at comparable P–T–X(fluid) conditions (Budanov and Shmulovich 2000). Results of these studies provide important constraints on the speciation of dissolved silica in aqueous solution at high P and T.

Experimental and analytical techniques

All runs were conducted in internally heated pressure vessels (modified after Ford 1972) using an argon pressure medium. Pressures were measured using manganin gauges calibrated periodically against the freezing point of mercury and the melting point of NaCl, and against a Heise pressure gauge, and are considered to be accurate to ± 5 MPa. Pressure uncertainties take into account small leakages of argon, which were usually < 10 MPa. Temperatures were measured using two Pt/Pt13%Rh thermocouples, one at either end of the capsule, and temperature gradients were controlled by tilting of the pressure vessels. Temperature uncertainty is typically within ± 2 °C, which reflects the thermal gradients in runs (see below). Where uncontrolled changes in thermal gradient occurred, runs were ignored (e.g. Q15, Q16, Table 2). Quenching was achieved by switching off the power, with temperatures < 100 °C being reached within 2–5 min. The fugacities of hydrogen and oxygen in the experiments were unbuffered, but the bomb walls exert a buffering influence on water-bearing charges between Ni–NiO and Fe_2O_3–Fe_3O_4.

High P–T mineral solubilities were measured from the weight change of single crystals using a rapid-quench method modified after Manning (1994). Experiments were conducted using a double Pt capsule arrangement. The small (3 mm diameter) inner capsule with perforated walls contained a single quartz or albite crystal. The large outer capsule (4 mm diameter × 20 mm length), enclosing the inner capsule, contained distilled H_2O and reagent grade NaCl (or oxalic acid, as a CO_2 source). Optically clear quartz crystals of approximate dimensions ~ 1.5×1×3 mm were cut from a large synthetic crystal (VNIISIMS, Aleksandrov, Russia). Albite crystals of similar size to the quartz were broken from a pure, natural low albite [< 1 mol% K-feldspar, Δ131 ~1.20 (Cu K_α); see Shmulovich and Graham 1996 for analysis], and sharp edges and corners were removed by cutting or grinding in order to protect capsule walls. Crystals were ultrasonically cleaned for ~1 min in distilled water prior to loading into capsules. SEM imaging showed the surfaces of crystals to be unmodified by ultrasonic cleaning. Inner capsules fitted tightly around the crystals in order to minimise the free volume and thus minimise precipitation of quench phases because mineral solubility decreases dramatically at the crystal surfaces during rapid cooling of runs to room temperature. For some albite crystals with perfect cleavage, which fractured during runs, the inner capsule also preserved the crystal for weighing. Cracking and fracturing of the crystals often took place, especially in runs with NaCl concentrations above halite saturation at room conditions.

Capsules were placed in the Ta capsule holders, and the thermal gradient along the outer capsule was regulated by tilting of the pressure vessel in order to establish the minimum temperature in the region of the crystal in the inner capsule, while the opposite end

of the capsule was overheated by 2–4 °C. As mineral solubility has positive temperature dependence, the temperature gradient eliminates mass transport to cooler parts of the fluid volume in the outer capsule. Capsules were initially compressed at room temperature and the pressure was then increased by heating.

Inner capsules were weighed before and after runs. After runs, the large capsules were weighed and cut open to extract the solution and any quench phase(s). The inner capsules were washed, dried, weighed, and then carefully opened in order to weigh the crystal by itself. Experience showed that weights of crystals were unreliable because extraction of the crystal (especially albite) from the inner capsule was often accompanied by loss of small non-quench particles (see below). Results based on weighing the entire inner capsules were found to be more reproducible, and are considered representative of weight loss arising from true crystal solubility. Thus the inner capsule protects the charge. Weighing errors include both a random (Gaussian) and a systematic component. Random weighing errors caused by balance sensitivity are $\sim \pm 0.01$ mg, and the reproducibility of measurements is near 0.02 mg. Calibration of crystal weights before and after runs was made at each weighing using pieces of Pt wire close in weight to the crystals. The relative weighing error depends on weight loss, and increases with decreasing $X(H_2O)$. For pure H_2O the relative error is $< 0.5\%$, whereas for low $X(H_2O)$ it is $\sim 5\%$.

In this rapid-quench method, the large decrease in mineral solubility on termination of experiments precipitates abundant quench phase(s) in the outer capsule. The identity, composition and proportions of quench phase(s) constrain the composition of the dissolved components of the fluid at high P and T, permitting the distinction of congruent versus incongruent dissolution. Solid run products were examined and analysed using a Philips XL30CP Analytical Scanning Electron Microscope fitted with an Oxford Instruments Link ISIS energy dispersive detector.

The solubility of Pt in H_2O–NaCl fluid was not measured. From experimental data at 500 °C and 0.1 GPa in NaCl solutions at fO_2 defined by the MnO–Mn_3O_4 buffer, log (Pt concentration) $= -3.4$ (g Pt/l) (Plyusnina et al. 1997). This value decreases with decreasing T and fO_2. No visible marks of Pt solution and transport were observed on the inner surfaces of capsules after runs with high concentrations of NaCl.

The overall precision of solubility measurements arises from several sources of error. Uncertainty in temperature measurement (± 2 °C) contributes $\sim 1\%$ errors in solubility, while uncertainties in pressure measurement (± 5 MPa) contribute errors of $\sim 1.5\%$. Random weighing errors are $\sim \pm 0.01$ mg, whereas relative errors (< 0.5–5%; see above) increase with decreasing $X(H_2O)$. Reproducibility of solubility measurement in repeat runs with the same fluid, such as runs Q33 and Q36 (Table 1) which differ by 0.02 mol% SiO_2, is equivalent to $\sim 10\%$ relative.

Table 1 Results of quartz solubility experiments. ΔS is the measured weight change of crystal during dissolution experiment. S is the solubility of quartz (g/kg H_2O) calculated from the initial wt H_2O and ΔS

Run	Time (h)	Initial NaCl or CO_2 (wt%)	H_2O (mg)	ΔS (mg)	S (g/kg H_2O)	Run product compositions			
						(mol%) H_2O	(mol%) NaCl	(mol%) CO_2	(mol%) SiO_2
(a)	H_2O–NaCl								
	0.9 GPa, 800 °C								
Q1	48	0	103.54	7.62	73.6	97.84	0	0	2.16
Q3	50	6.9	101.35	7.2	71	95.78	2.18	0	2.04
Q4	50	20.4	94.38	5.92	62.7	91.1	7.19	0	1.71
Q5	48	42.7	73.6	3.98	53.8	80.28	18.43	0	1.29
Q10	75	48.26	74.54	2.53	33.9	77.07	22.14	0	0.78
Q11	72	20.4	96.98	5.49	56.6	91.25	7.2	0	1.55
Q23	50	60	45.23	2.2	48.7				
Q29	38	76	33.72	0.52	15.4	50.5	49.26	0	0.23
Q30	38	80	25.69	0.29	11.3	44.73	55.11	0	0.16
Q31	38	70.3	45.88	0.98	21.4	57.62	42.01	0	0.37
	0.9 GPa, 900 °C								
Q32	12	0	89.34	11.24	125.8				
	0.9 GPa, 650 °C								
Q12	70	0	105.4	2.82	26.7	99.21	0	0	0.79
Q13	70	0	116.78	3.13	26.8	99.2	0	0	0.8
Q14	72	48	54.31	0.71	13.1	77.62	22.07	0	0.31
Q20	65	0	102.76	2.93	28.5	99.15	0	0	0.85
Q21	65	20.4	61.61	1.46	23.7	91.23	8.12	0	0.65
	0.9 GPa, 500 °C								
Q17	92	0	102	1	9.8	99.71	0	0	0.29
Q18	92	20.4	89.61	0.73	8.1	91.62	8.15	0	0.22
Q19	92	38.6	81.4	0.13	1.6	83.74	16.22	0	0.04
	0.5 GPa, 800 °C								
Q25	64	0	77.3	3.92	50.7	98.5	0	0	1.5
Q26	64	24.9	92.11	2.85	41.2	89.73	9.16	0	1.11
Q27	62	48.1	70.08	2.1	30	77.26	22.05	0	0.69
Q28	62	68.3	48.26	0.93	19.3	59.9	39.75	0	0.35
(b)	H_2O–CO_2								
	0.9 GPa, 800 °C								
Q33	60	0	28.26	0.29	10.26	49.92	0	49.92	0.16
Q34	65	0	59.49	1.03	17.31	64.82	0	34.85	0.33
Q35	65	0	58.68	1.25	21.3	70.27	0	29.28	0.45
Q36	62	0	30.49	0.38	12.46	49.91	0	49.91	0.18
Q37	62	0	83.13	2.97	35.73	83.54	0	15.57	0.89

Results

Results of experiments on quartz solubility are presented in Table 1 and those on albite and diopside dissolution in Table 2.

Quartz

Quartz solubility was measured in H_2O–NaCl fluids at 0.9 GPa and 500, 650, 800 and 900 °C, and at 0.5 GPa and 800 °C, and in H_2O–CO_2 fluids at 800 °C and 0.9 GPa. Reproducibility is demonstrated by three repeated data points (Table 1): runs Q4 and Q11 in H_2O–NaCl fluid, runs Q12, Q13 and Q20 in pure water, and runs Q33 and Q36 in H_2O–CO_2 fluid. Comparable solubilities measured for different run times indicate that measured solubilities approach equilibrium values. Run times were comparable to those of Manning (1994) and Newton and Manning

(2000), in which attainment of equilibrium values was also demonstrated.

The concentration dependence of quartz solubility in H_2O–NaCl fluid at different temperatures and 0.9 GPa is shown in Fig. 1a. Results at 800 °C in both fluid mixtures studied, and at 0.9 and 0.5 GPa, are compared in Fig. 2. Our new results are in good agreement with those of Manning (1994) for pure H_2O and of Newton and Manning (2000) for H_2O–NaCl and H_2O–CO_2, demonstrating the consistency of the experimental techniques. Two results at 800 °C and 0.9 GPa (Q5 and Q23), in which changes in the thermal gradient during the runs caused the coolest part of the capsule to move away from the vicinity of the quartz crystals, are inconsistent with other 800 °C results, probably as a result of mass transport. These anomalous results illustrate the sensitivity of the method to the establishment of the correct thermal regime around the crystals.

Within experimental error, quartz solubility at 0.9 GPa appears to decrease linearly with increasing NaCl concentration (in mass%) at each temperature

Table 2 Results of albite, diopside solubility experiments. ΔS is the measured weight change of crystal during dissolution experiment. S is the solubility (g/kg H_2O) calculated from the initial wt H_2O and ΔS
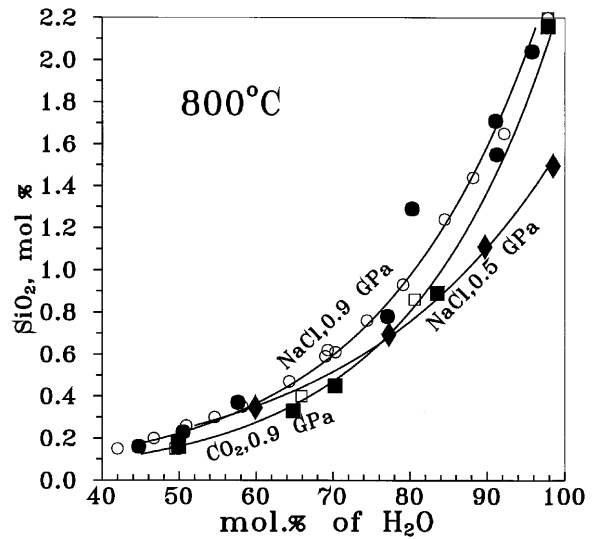
| Run	Time (h)	NaCl (wt%)	H_2O (mg)	ΔS (mg)	S (g/kg H_2O)	Remarks
(a) Albite in H_2O–NaCl						
	0.9 GPa, 650 °C					
Ab1	32	0	101.3	5.72	56.5	
Ab2	46	20.4	119.38	1.92	20.1	
Ab3	46	49.96	52.29	1.5	28.7	
Ab8	65	20.4	102.5	4.74	50.7–54	Transport
Ab9	65	54.74	63.08	0.56	8.7	
Ab10	54	24.9	93.97	1.67	17.8	
Ab11	54	6.9	96.46	2.94	30.5	
Ab15	48	0	78.26	4.58	58.6	
Ab16	48	0	79.95	4.65	58.2	
	0.9 GPa, 500 °C					
Ab5	92	0	82	1.84	22.4	
Ab6	92	49.7	56	1.75	21.6	
Ab7	92	20.4	65.7	0.37	6.5	
	0.9 GPa, 800 °C					
Ab12	50	55.3	52.78	1.8	34	
Ab13	50	67.7	53.8	1.34	25	
Ab17	38	0	94.46	9.48	100.3	
Ab18	24	24.9	95.99	4.59	47.8	
Ab19	24	6.9	98.5	8.83	89.6	
	0.9 GPa, 900 °C					
Ab20	16	0	94.12	16.8	178	
Ab21	14	0	95.44	18.69	195.8	
Ab22	14	0	91.95	16.65	181	
	0.5 GPa, 650 °C					
Ab14	110	59.13	59.55	0.41	6.9	
Ab23	110	0	101.91	1.84	18	
Ab24	112	24.9	89.03	0.84	9.4	
Ab25	112	80.95	24.77	0.76	30.7	Transport
(b) Albite in H_2O–CO_2						
	0.9 GPa, 800 °C					
Ab26	60	71(CO_2)	34.41	0.16	4.6	
(c) Diopside in H_2O–NaCl						
	0.5 GPa, 650 °C					
Di-1	122	0	106.9	0.05	0.5	
Di-2	122	53.22	75.07	0.41	5.5	
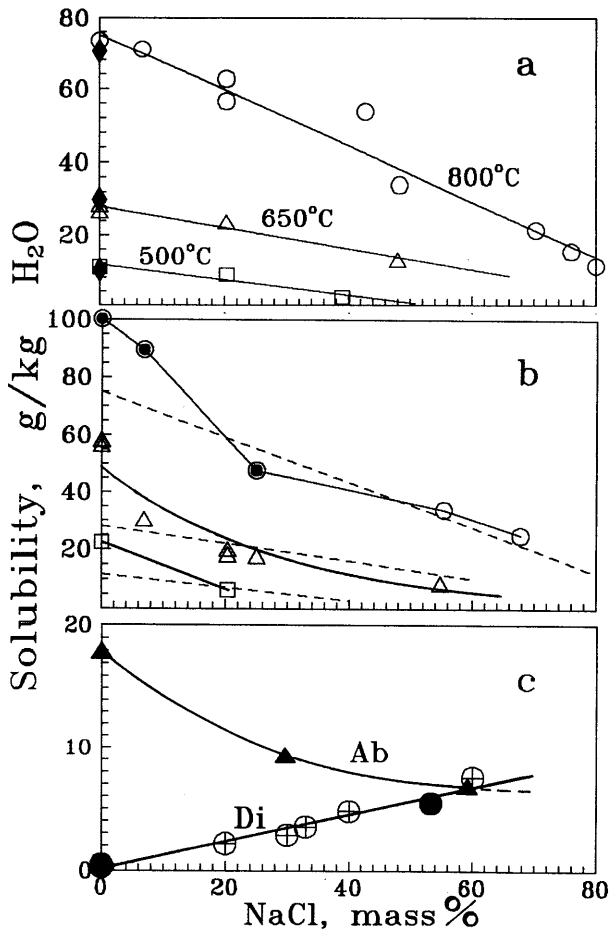
Fig. 1 Experimental results of mineral solubilities in H_2O–NaCl fluids plotted as function of mass% NaCl. **a** quartz solubility at 0.9 GPa (9 kbar) and 800 °C (*open circles*), 650 °C (*open triangles*) and 500 °C (*open squares*); *diamonds* are data of Manning (1994) on quartz solubility in H_2O under same P–T conditions; **b** albite solubility at 0.9 GPa (9 kbar) and 800 °C (*open circles*), 650 °C (*open triangles*) and 500 °C (*open squares*); the trends from the quartz results (**a**) are shown for comparison; *double circles* are runs where albite melted; **c** diopside and albite solubility at 0.5 GPa (5 kbar) and 650 °C; *filled circles* this study; *open circles with cross* data of Budanov and Shmulovich (2000). Note albite and diopside solubilities are 'apparent' solubilities because dissolution is incongruent

Fig. 2 Experimental results for quartz solubility at 800 °C and 0.5 GPa (*diamonds*) and 0.9 GPa (*filled circles*) in H_2O–NaCl, and at 800 °C and 0.9 GPa in H_2O–CO_2 (*filled squares*) fluids; concentrations in mol%. Data of Newton and Manning (2000) at 800 °C and 1.0 GPa for H_2O–NaCl (*open circles*) and H_2O–CO_2 (*open squares*) shown for comparison. Note similarity of solubilities at 0.9 GPa, close to experimental uncertainties, irrespective of fluid type
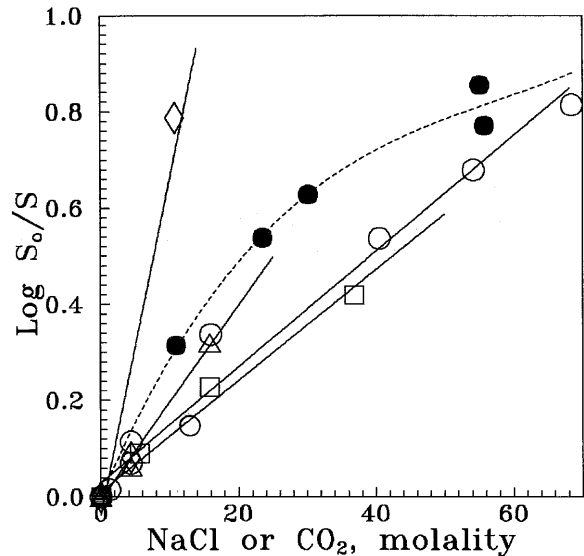
Fig. 3 Fit of quartz solubility data for H_2O–NaCl (*open symbols*) and H_2O–CO_2 (*filled circles*) fluids to the Setchenow equation (see text) where S_o and S are the molal solubilities of silica in pure H_2O and H_2O–NaCl (or H_2O–CO_2) solution respectively. *Open symbols* H_2O–NaCl; *circles* 0.9 GPa, 800 °C; *squares* 0.5 GPa, 800 °C; *triangles* 0.9 GPa, 650 °C; *diamonds* 0.9 GPa, 500 °C; *filled circles* H_2O–CO_2 at 0.9 GPa, 800 °C

(Fig. 1a). Comparison of solubilities at 0.5 and 0.9 GPa (Fig. 2) demonstrates that the relative change of quartz solubility with changing salt concentration is much greater at the higher pressure. In NaCl-rich brines quartz solubility does not change with pressure at the P–T conditions of our experiments, whereas at low X(NaCl) solubility at 0.9 GPa is approximately double the solubility at 0.5 GPa (Fig. 2). The dependence of quartz solubility on the compositions of H_2O–NaCl and H_2O–CO_2 fluid at 800 °C and 0.9 GPa is also compared in Fig. 2. Both curves show a very similar decrease in solubility with decreasing X(H_2O), with solubility in H_2O–NaCl being slightly larger.

From Fig. 2, the dependence of quartz solubility S (as mol% SiO_2) on concentration of H_2O

[$C(H_2O)$] in mol% at 800 °C may be described by the equation:

$$S = A \, exp \, [B * C(H_2O)]$$

For the system H_2O–NaCl, $A = 0.0215$, $B = 0.0475$ at 0.9 GPa; $A = 0.03585$, $B = 0.0381$ at 0.5 GPa; for H_2O–CO_2 at 0.9 GPa, $A = 0.0111$, $B = 0.0535$.

In summary, the main features of our results on quartz solubility are: (1) solubilities in both H_2O–NaCl and H_2O–CO_2 fluids are still quite measurable at water concentrations below 50 mol%; (2) quartz solubility in H_2O–NaCl is dependent on pressure at high water concentrations ($> \sim 75$ mol% H_2O), whereas near $X(H_2O) = 0.5$ solubility is essentially the same at 0.5 and 0.9 GPa (Fig. 2); (3) solubility of quartz in H_2O–NaCl and H_2O–CO_2 fluids at 0.9 GPa is similar at all $C(H_2O)$, with solubility in H_2O–NaCl being larger; (4) all solubility data approximate exponential functions of $X(H_2O)$ (Fig. 2). These observations must all be accounted for in any thermodynamic model of quartz dissolution.

The solubility of a non-electrolyte such as silica in an aqueous salt solution under low P–T conditions can typically be fitted by the Setchénow relationship:

$$\log\left(\frac{So}{S}\right) = Dm$$

where So and S are the molal solubilities of silica in pure water and salt solution respectively, and m is the molality of salt. D is a constant whose value depends on temperature and the particular salt. Quartz solubility data for H_2O–NaCl fluids at 800 °C and 0.9 and 0.5 GPa are plotted as log (So/S) vs m in Fig. 3, yielding a slope of value D for the appropriate P–T conditions. These high-P–T data show a good linear correlation for the electrolyte (salt) solution, as for low-P amorphous silica data (Chen and Marshall 1982; Marshall and Chen 1982), but not for the non-electrolyte (H_2O–CO_2) fluid. Any effect of pressure on the value of the Setchénow constant (D) is within experimental error, and D at 800 °C is ~ 0.013.

Albite

Since the dissolution of albite is not strictly congruent (Anderson and Burnham 1983; see discussion below), the weight change of albite crystals in our experiments did not measure the solubility of albite sensu stricto, but rather the solubility of a new equilibrium mineral assemblage which included not only albite but the new mineral phase(s) precipitated (cf. Woodland and Walther 1987). The presence of additional solid phase(s) limits the extent of dissolution of albite. We use solubility here as an apparent solubility measured by the weight loss of albite crystals. Our objectives were to measure the relative changes in albite solubility and the identity of additional solid plus quench phases with varying $X(NaCl)$, to compare quartz and albite solubilities at any $X(NaCl)$, to examine the congruence/incongruence of the dissolution reaction, and to constrain the composition and possible speciation of the fluid in equilibrium with the solid assemblage.

Albite solubility was measured in H_2O–NaCl fluids at 0.9 GPa (500–900 °C) and 0.5 GPa (650 °C), and in H_2O–CO_2 fluids at 0.9 GPa (900 °C). The results demonstrate more complicated behaviour than for quartz,

but initial runs in saline fluids indicate that albite solubility is of the same order of magnitude as that of quartz (Fig. 1b), i.e. tens of grams per kilogram of water at 0.9 GPa and 500–900 °C. By contrast, quartz solubility at room temperature is $\sim 10^{-7}$ g/kg H_2O.

Solubilities of albite are presented in Table 2 and Fig. 1b. Runs Ab8 and Ab25, which showed evidence of mass transport after the thermal gradient changed during runs, are excluded from Fig. 1b. Solubilities of albite and quartz, and their dependence on $X(NaCl)$, are indistinguishable except at $X(NaCl) < 0.05$ where albite solubility is higher at both 0.5 and 0.9 GPa. At 0.9 GPa, albite is molten at 800 °C in water-rich fluid (Goldsmith and Jenkins 1985), and the measured solubility is that of the hydrous melt.

Incongruent versus congruent dissolution of albite

Previous studies have reported at least qualitative evidence (presence of Al-rich product phases) for incongruent dissolution of albite in H_2O under hydrothermal conditions (Currie 1968; Davis 1972; Anderson and Burnham 1983), with paragonite forming as a dissolution reaction product, Na/Al greater than the stoichiometric (albite) value, and Si/Na equal to the stoichiometric value. Shmulovich and Graham (1996) reported that amorphous spheres of silicate material quenched from aqueous fluids coexisting with albite and/or albite melts at 0.9 GPa, 700–900 °C, were close to stoichiometric albite in composition (see also Paillat et al. 1992; Webster et al. 1992a, 1992b). Stalder et al. (2000) investigated albite solubility in water between 0.5 and 1.5 GPa, and reported a bulk solubility of 2.1 wt% at 720 °C and 1.0 GPa. Element ratios were determined from analysis of quenched fluid in a diamond powder trap and indicated enrichment of silica in the fluid phase. At 0.5 GPa, Na/Al in the fluid exceeded the stoichiometric value, but at 1.0 and 1.5 GPa this effect was reversed. Thus previous studies indicate that the albite solute is quite close to stoichiometric albite in composition over a wide range of P and T.

In this study, albite dissolved incongruently, with formation of secondary phases, under most run conditions. The products of incongruent dissolution formed as plates on the surface of the albite crystal in the inner capsule (below). Products of runs with pure water, or with NaCl solutions that were undersaturated at room P and T, differed from those with saturated brines. In the latter case, the secondary phase(s) formed after incongruent dissolution were largely or completely removed during washing to remove precipitated halite. For this reason, secondary phases were only investigated for runs with relatively low salinity fluid.

Run products at 500 and 650 °C in NaCl-free fluids showed evidence of secondary phase formation on albite crystal surfaces, indicating incongruent dissolution. X-ray diffraction and analytical SEM investigations (Fig. 4) showed very thin plates of secondary paragonite and
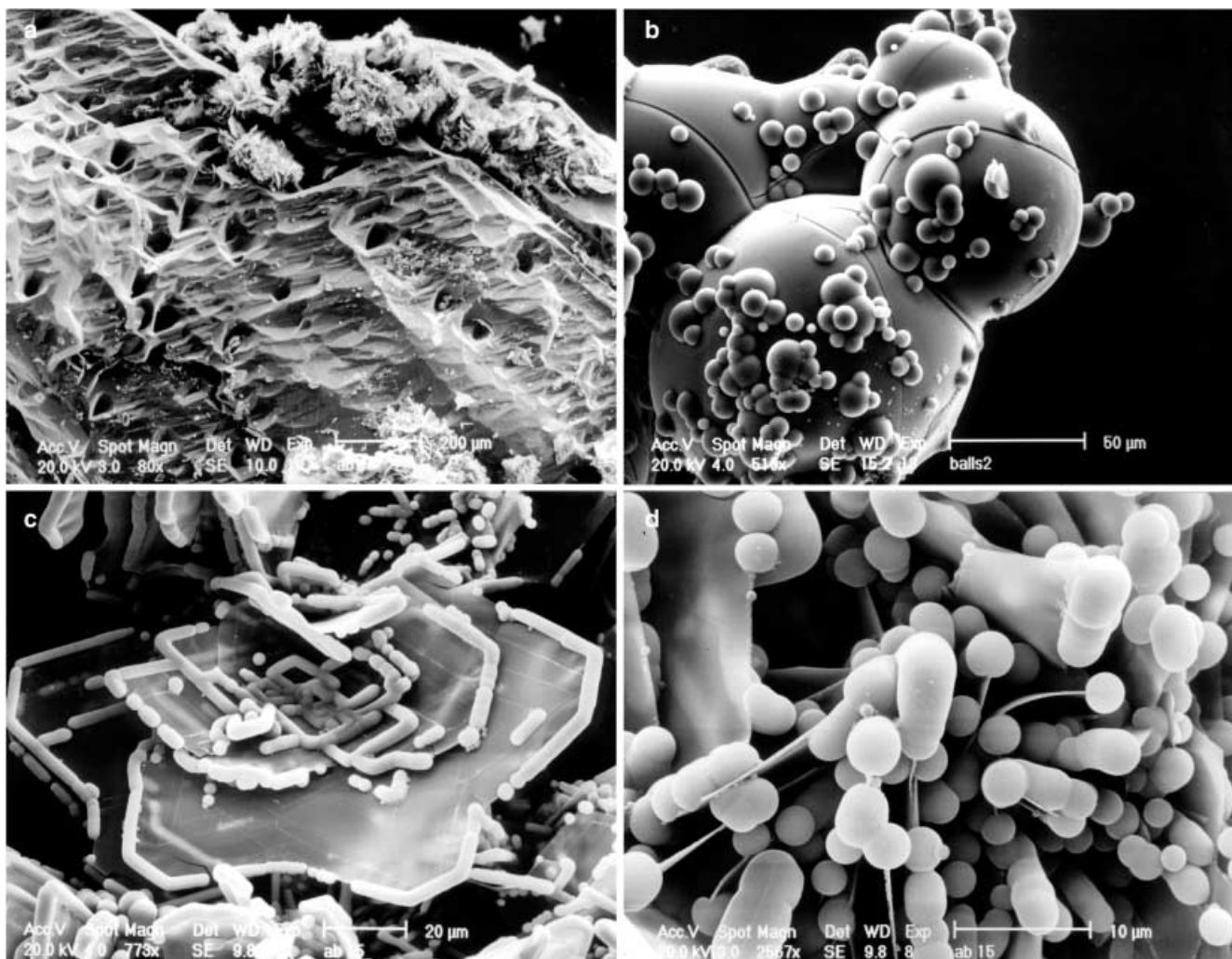
Fig. 4 SEM images of secondary reaction products of incongruent albite dissolution in H_2O at 0.9 GPa. **a** Albite crystal surface in run Ab15 at 650 °C showing clusters of mica; spheres of quench material did not precipitate inside the inner capsule; **b** large spheres of albite melt decorated with small spheres of Al-depleted quench material in run Ab17 at 800 °C; **c** thin paragonite plates decorated by spheres and rods of quench albite glass in run Ab15; **d** thin paragonite plates attached to spheres of quench glass (run Ab15)

Na-margarite, whereas quench products were small spheres close to albite in composition that never wetted the surfaces of albite crystals or plates of secondary mica, but precipitated mainly within the large outer capsules. Wetting by quenched albite glass was observed along the edges of the mica plates, where they formed both as spheres and rods (Fig. 4c, d).

We weighed the albite crystal from run Ab15 with and without the thin crust of secondary minerals. In spite of visible mica crystals on the surface of albite and amongst quench phases in the large outer capsules, the weight difference between the two crystals was not more than 0.1 mg including the quenched material precipitated on paragonite and inside the inner capsule. The quantity of secondary material was also estimated

visually from SEM images (Fig. 4). The dissolution of albite at 0.9 GPa is therefore close to congruent, with an additional component of incongruent dissolution releasing metasilicate (Na_2SiO_3) to leave a NaAl-mica residue.

Quenched solutions from runs with albite mono-crystals were transparent with both pure water and salt solutions, suggesting that supersaturation or colloid concentration after quench were negligible. Quench products from runs with highly saline fluids (e.g. Ab12) were spheres with atomic ratios Na:Al:Si = 1.2:0.95:3, close to albite stoichiometry, but with a small enrichment in sodium and depletion in Al consistent with formation of Na-micas observed on the surface of albite crystals. The presence of excess Na in solution limits the solubility of albite, and the stability of NaAl micas indicates that the system was undersaturated in silica.

Further evidence for albite dissolution being close to congruent at 0.9 GPa comes from comparison of albite and quartz solubilities in pure H_2O at 0.9 GPa and the same temperature conditions (500–900 °C). Albite and quartz solubilities are plotted against each other in Fig. 5, yielding a correlation that approximates to:
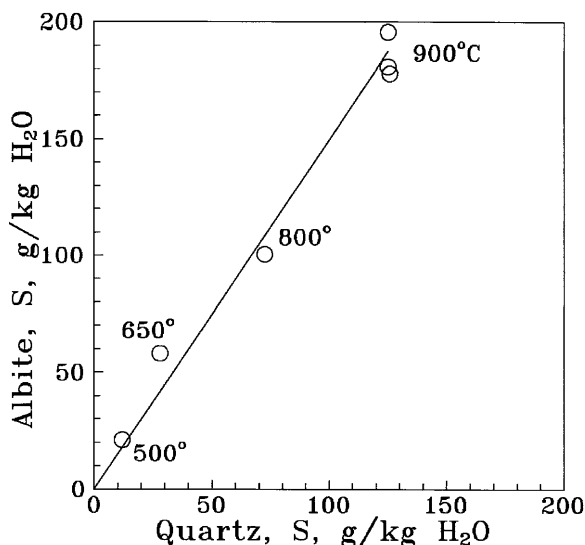
Fig. 5 Comparison of the solubilities (S) of albite and quartz at 0.9 GPa in pure water. The significance of the slope is discussed in the text

$$S(Ab) = 1.5 * S(Q)$$

where S is solubility in grams per kilogram H_2O. If albite dissolution were completely congruent, dissolution of 1.46 g albite would yield 1 g SiO_2 in solution. This result shows excellent agreement with the slope in Fig. 5, indicating that the yield of silica from albite/albite melt dissolution is probably close to congruent in pure water from 500–900 °C at 0.9 GPa.

Our results confirm and amplify the observation (e.g. Anderson and Burnham 1983; Shmulovich and Graham 1996) that fluids in equilibrium with albite are close to stoichiometric albite in composition over a wide range of P and T. This has implications for the speciation of Na, Al and Si in aqueous solution. Si is known to form hydrated complexes in aqueous solution (e.g. Walther and Orville 1983; Zotov and Keppler 2000; see below). However, the dissolved SiO_2 from albite dissolution at 500–600 °C is reported to be greater than the solubility of quartz at pressures above ∼0.7 GPa (Davis 1972; Anderson and Burnham 1983), even though quartz did not form in the albite dissolution experiments. Therefore, some SiO_2 from albite dissolution must be in a form other than hydrated silica. Woodland and Walther (1987) showed that Al dissolves dominantly as a Na–Al complex in fluids in equilibrium with albite, paragonite and quartz at 350–500 °C, 0.1–0.25 GPa, and this complex may contribute to the remarkable constancy of fluid composition. The excess of Na over Al relative to albite stoichiometry also requires additional Na–Si complexing. Another interpretation of these experimental results is that the dominant dissolved species in aqueous solution has a hydrated feldspar stoichiometry (with minor additional Na-metasilicate species). Further resolution of this problem requires independent experimental verification by direct in-situ methods.

The other remarkable feature of our results is the much larger effect of changing $X(NaCl)$ on albite versus quartz solubility at low $X(NaCl)$ such that the apparent and actual solubilities of albite and quartz (g/kg) respectively, and their dependence on $X(NaCl)$, are indistinguishable except in H_2O-rich fluids [$X(NaCl) < 0.05$; Fig. 1]. The composition of dissolved species, as judged by analysis of quenched spheres, remains broadly albitic in composition in pure H_2O (Shmulovich and Graham 1996) and at high $X(NaCl)$ (run Ab12; see above; see also Anderson and Burnham 1983); however, for pure H_2O at 0.9 GPa this composition is close to stoichiometric albite, whereas at high $X(NaCl)$ it is relatively enriched in Na and depleted in Al. Na mica(s) form at various $X(NaCl)$. Thus increasing $X(NaCl)$ leads to measurable change in the composition of dissolved species, with in particular a decrease in Al, and, by inference, in Na–Al complexing.

An original objective of this study was to explain why, under the same P–T–X(fluid) conditions, water activities in the H_2O–CO_2–NaCl system calculated from feldspar-melting experiments are smaller than those calculated from displacement of the brucite–periclase–H_2O equilibrium (Aranovich and Newton 1996, 1997; Shmulovich and Graham 1996) and from phase equilibria in the system H_2O–CO_2–NaCl measured from synthetic fluid inclusions in quartz (Shmulovich and Graham 1999). One suggested explanation of this discrepancy was the enhanced solubility of feldspars compared with quartz or brucite–periclase in aqueous salt solutions under subcritical P–T conditions. However, the solubilities of quartz and feldspar are indistinguishable in H_2O–NaCl fluids except at very low $X(NaCl)$ (Fig. 1), and thus the discrepancy is not explained by differential mineral solubilities. An explanation remains elusive.
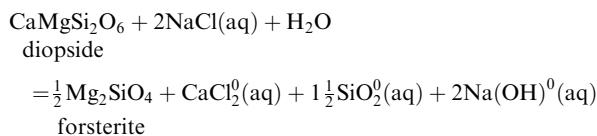
Diopside

Diopside solubility (again an apparent solubility, because of incongruent dissolution) was measured by Budanov and Shmulovich (2000) using a cold-seal pressure vessel at 650 °C, 0.2–0.75 GPa. Two further experiments were conducted in the present study at 0.5 GPa and 650 °C in an internally heated pressure vessel, in order to compare the results. As shown in Fig. 1c, diopside solubility increases with increasing salt content of the fluid (salt-in effect) at all pressures studied (0.2, 0.5 and 0.75 GPa) because of the absence of a common ion. Diopside solubility is in fact almost negligible in pure water but increases linearly with increasing salinity to reach similar values to those of quartz and albite in concentrated brines (> 50 mass% NaCl).

The solution behaviour of diopside in NaCl solution may be readily explained. Ca and Mg are both complexed by Cl in aqueous solution, and hence their concentrations will increase with increasing Cl. However, exchange of divalent cations for Na and Cl ion pairs will

lead to an increase in the NaOH content of the fluid, which itself enhances silica solubility. The main species in solution are those of Ca and Si (Budanov and Shmulovich 2000), with extremely low concentrations of Mg because of the low solubilities of Mg-silicates. We can write the following reaction for incongruent dissolution of diopside:

$$CaMgSi_2O_6 + 2NaCl(aq) + H_2O$$
$$\text{diopside}$$
$$= \tfrac{1}{2}Mg_2SiO_4 + CaCl_2^0(aq) + 1\tfrac{1}{2}SiO_2^0(aq) + 2Na(OH)^0(aq)$$
$$\text{forsterite}$$

where $Na(OH)^0(aq)$ may react further with $SiO_2^0(aq)$ to form additional silica species at high pH. Forsterite (Mg_2SiO_4) was not the only secondary phase that precipitated on diopside surfaces after incongruent dissolution. Analytical SEM also indicated the presence of talc and/or serpentine as well as wollastonite, but the latter may have been a quench precipitate. Thus diopside dissolved incongruently in both water and NaCl solutions.

Speciation of dissolved silica in aqueous solution at high P and T

Background and previous work

Minerals dissolve in aqueous fluids through the formation of ions, ion pairs or aqueous complexes that may be charged or neutral. The identity and charge of these species depend on pressure, temperature and the composition of the fluid. At the high pressures and temperatures of this study, high density aqueous electrolytes at low concentrations become strongly dissociated into simple ionic species, reflecting changes in the dielectric constant of water (Quist and Marshall 1968; Helgeson and Kirkham 1974; Marshall and Franck 1981; Frantz and Marshall 1982). These ions become solvated by water molecules, with ordering into hydration shells and reduction of water activities relative to ideal mixing (Shmulovich et al. 1982; Aranovich and Newton 1996; Shmulovich and Graham 1996, 1999). Models of speciation in aqueous solutions, such as H_2O–CO_2 and H_2O–NaCl, are based on measurements in dilute solutions, ranging up to about 4–6 molar. However, H_2O–NaCl fluid compositions used in this and earlier studies (e.g. Shmulovich and Graham 1996, 1999; Newton and Manning 2000) range up to ~50 molar and are hydrosaline melts. The speciation in such concentrated fluids is unknown, although Oelkers and Helgeson (1990) have proposed the formation of polynuclear complexes such as Na_2Cl^+ and $NaCl_2^-$. Variation of speciation with $X(H_2O)$ might be expected as in H_2O–CO_2 fluids. Aqueous solutions of polar and non-polar molecules such as H_2O–CO_2 may be described as mixtures of simple molecules, especially for P–T conditions of complete miscibility.

Current models of silica speciation in aqueous solution are largely based on thermodynamic interpretation of experimental quartz solubility data at low pressures. The solvation of silica in aqueous solution during quartz dissolution experiments has usually been represented by the generalised reaction:

$$SiO_2(Qtz) + n\,H_2O = SiO_2 \cdot n\,H_2O \tag{1}$$
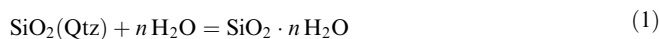
(e.g. Walther and Helgeson 1977; Walther and Orville 1983; Walther 1991) where n is the hydration number of silica, and the product of reaction represents the dominant uncharged hydrated (solvated) silica species. Writing $SiO_2{\cdot}nH_2O$ as $SiO_2(aq)$ we obtain for equilibrium (1) for any value of n:

$$K_n = \frac{aSiO_2(aq)}{(aH_2O)^n} \tag{2}$$

$$\log K_n = \log aSiO_2(aq) - n.\log aH_2O \tag{3}$$

Assuming that (1) reaction (1) represents the dissolution of quartz; (2) dissolved silica does not complex with fluid species other than H_2O; and (3) the same hydrated silica species is predominant across a range of fluid compositions, then the hydration number n can in principle be determined using Eq. (3) from the slope of a plot of $\log aSiO_2(aq)$ vs. $\log a(H_2O)$. The degree of solvation of hydrated aqueous silica [i.e. the value of n in Eqs. (1)–(3)] has been constrained by experimental quartz dissolution data in pure water (Anderson and Burnham 1965; Sommerfeld 1967; Crerar and Anderson 1971; Shettel 1974; Walther and Helgeson 1977, 1980) and more recently in H_2O–CO_2 and H_2O–Ar solutions at low pressures (Anderson and Burnham 1967; Novgorodov 1975; Walther and Orville 1983). These results (reviewed by Walther and Helgeson (1977) and Walther and Orville (1983)) suggest that silica dissolves primarily as variably hydrated monomeric $Si(OH)_4$ tetrahedra. Independent support for this interpretation has been provided by in-situ Raman spectroscopy of H_2O–SiO_2 fluids at high P and T (Zotov and Keppler 2000; see below).

Thermodynamic analysis of data on quartz solubility in H_2O–CO_2 fluids up to pressures of 0.5 GPa (Walther and Orville 1983; Fig. 4) indicates a hydration number close to 4, and hence that the dominant dissolved hydrated silica species has the composition $SiO_2.4H_2O$. Limited data at low $X(H_2O)$ (Novgorodov 1975) point to a decrease in n to <3 at low $X(H_2O)$ (Walther and Orville 1983), indicating that the degree of solvation may vary with fluid composition in addition to P and T. Newton and Manning (2000) interpreted their quartz solubility data for H_2O–CO_2 fluids at 1 GPa, 800 °C to indicate that n varies from 5 at low $X(CO_2)$ to ~3 at $X(CO_2) = 0.67$.

The stereochemistry of silica complexes in aqueous solution imposes some constraints on possible values of the hydration number n. Walther and Orville (1983) interpreted a silica hydration number of 4 for H_2O–CO_2 fluids in terms of a silica complex $Si(OH)_4{\cdot}2H_2O$, in which silicon is tetrahedrally co-ordinated by hydroxyls and two additional water molecules are hydrogen bonded to the hydroxyl oxygens.

Alternative, independent constraints on the structure and speciation of aqueous silica have recently been provided by in-situ laser Raman spectroscopy of a saturated solution of quartz in pure H_2O of density 0.94 up to 900 °C and 1.4 GPa, overlapping the conditions of the present study (Zotov and Keppler 2000). Results confirm the dominance of $Si(OH)_4$ at the P–T conditions of the present study, but indicate significant polymerisation to form additional $H_6Si_2O_7$ dimers at higher pressures. However, the technique cannot detect hydrogen-bonded water molecules in surrounding hydration shells. The spectroscopic study thus provides general support for the existence of comparable dissolved silica species to those postulated from thermodynamic modelling of quartz dissolution data (reviewed above) under the high P–T conditions of the present study. Nonetheless, the hydration number necessarily provides a simplistic model of silica speciation that averages time-dependent short-range ordering, to constrain the dominant species. Other species may be present but remain unidentified by either spectroscopic or thermodynamic analysis, and thus the 'average' species may have a fractional hydration number.

With these provisos, we have used thermodynamic analysis to interpret the speciation in H_2O–CO_2 fluids at high pressures. We compare our results with those for lower pressure experiments, evaluate our results for the dissolution of silica in H_2O–NaCl in the light of results from H_2O–CO_2 experiments, and assess evidence for similarities or differences in the identity of dissolved silica species between different fluids and between high and low pressures.

Quartz solubility in H_2O–CO_2 fluids

Here, we use our experimental quartz dissolution data to estimate the degree of solvation of aqueous silica [i.e. the value of n in Eqs. (1)–(3)] at high pressures. Quartz solubility may be expressed in terms of either the molality or the mole fraction of SiO_2 in aqueous solution. Because $X(SiO_2)$ does not vary linearly with molality, differences between the two concentration scales become significant at high silica concentrations. Because of the very high solubility of quartz in water-rich fluids under the high pressure conditions investigated here, we have plotted silica solubility as $X(SiO_2)$ rather than using molality as is conventional in studies under less extreme conditions. The use of mole fraction rather than molality results in slightly higher calculated hydration numbers (e.g. Walther and Orville 1983).

In order to rigorously extract a value of n using Eq. (3), it would be necessary to evaluate activity coefficients (γ) for both water and aqueous silica in H_2O–CO_2 fluids. Activity models for H_2O–CO_2 fluids show small positive deviations from ideality ($\gamma(H_2O) > 1$; Kerrick and Jacobs 1981; Aranovich and Newton 1999; see also Shmulovich and Graham 1996, their Fig. 4). The use of mole fractions [$X(H_2O)$] rather than water activities [$a(H_2O)$] to fit our

data to Eq. (3), i.e. $\gamma(H_2O) = 1$, results in a shift of water 'activity' to lower values by up to > 0.1 log units, depending on fluid composition (see also Walther and Orville 1983). Resulting values of n are also reduced. There are, however, no data on the activity of aqueous silica [$aSiO_2(aq)$] in aqueous fluids. If we assume that there is a similar tendency for hydrated silica species to associate with water molecules in the fluid, this implies a similar positive deviation from ideality [$\gamma SiO_2(aq) > 1$] for silica in the fluid. For these reasons, we have plotted log $X(SiO_2)$ vs log $X(H_2O)$ to constrain the hydration number (n) of SiO_2, accepting that any residual (non-ideal) effects of interaction between aqueous silica species and water in the H_2O–CO_2 fluid are incorporated into the resulting value of n.

Results of a thermodynamic analysis of quartz solubility data from this study are presented in Fig. 6. While the overall slope of our experimental data for quartz solubility in H_2O–CO_2 is close to 3, a closer examination of these data indicates that the correlation is not linear, and the hydration number decreases with decreasing water activity, as inferred from the low pressure solubility data (Walther and Orville 1983). The data for the water-rich part of the range investigated approximate a value of $n = 4$, while for CO_2-rich fluids $n = 2$ may be a better approximation. These values imply that the dominant species are $Si(OH)_4 \cdot 2H_2O$ and [at low $X(H_2O)$], $Si(OH)_4$. This analysis indicates that the speciation of SiO_2 in H_2O–CO_2 fluids at 0.9 GPa varies with fluid composition and is essentially indistinguishable from that at lower pressures (Walther and Orville 1983), which is in agreement with recent high P–T experimental data (Newton and Manning 2000) and spectroscopic studies (Zotov and Keppler 2000). Newton and Manning (2000) calculated hydration numbers up to $n = 5$ for SiO_2 in H_2O–CO_2 fluids at 1 GPa, and the small
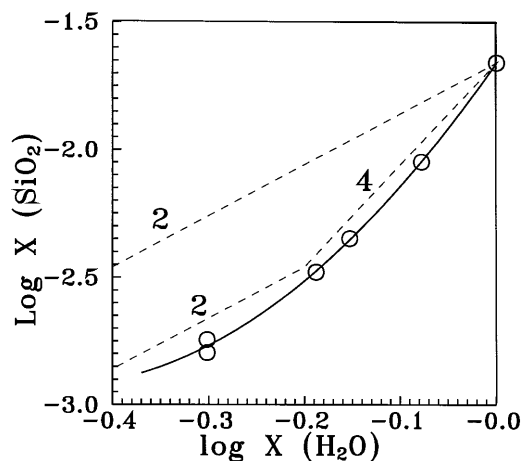
Fig. 6 Plot of log $X(SiO_2)$ vs. log $X(H_2O)$ [Eq. (3); see text for discussion] for quartz dissolution in H_2O–CO_2 at 0.9 GPa, 800 °C. *Solid curve* fits solubility data. *Dashed lines* are theoretical lines for $SiO_2 \cdot 4H_2O$ ($n = 4$) and $SiO_2 \cdot 2H_2O$ ($n = 2$), where n is the hydration number of the hydrated silica complex. Data points for water-rich fluids may be fit by a line of slope corresponding to $n = 4$, but in water-poor fluids $n = 2$ may be a better fit

discrepancy with the present study appears to result from their use of $a(H_2O)$ rather than $X(H_2O)$.

Quartz solubility in H_2O–NaCl fluids

Early work on quartz solubility in saline solutions (Xie and Walther 1993) was carried out at low pressures, where H_2O–NaCl mixing is near to ideal. However, water does not mix ideally in H_2O–NaCl fluids at the high-pressure conditions of our experiments (Aranovich and Newton 1996; Shmulovich and Graham 1996, 1999). In aqueous salt solutions containing dissolved silica at high pressures, dissociated Na^+ and Cl^- ions and dissolved silica species compete for available water in the fluid. In addition to these H_2O–NaCl and H_2O–SiO_2 interactions, there may also be significant interaction between Na^+ and Cl^- ions and H_2O in hydration shells around silica species. The solvation of water around dissociated Na^+ and Cl^- ions in aqueous salt solutions at high pressures and temperatures is inferred from high P–T phase equilibria and H_2O–NaCl activity-composition relations. This leads to negative deviations from ideality [$\gamma(H_2O)$ < 1] for water in high pressure brines, in contrast to the positive deviations from ideality [$\gamma(H_2O)$ > 1] in H_2O–CO_2 fluids at the same P and T. Newton and Manning (2000) compared the solubility of quartz in H_2O–NaCl vs H_2O–CO_2 fluids at 1 GPa and 800 °C using plots of $m(SiO_2)$ vs $a(H_2O)$, and concluded that quartz is up to an order of magnitude more soluble in concentrated H_2O–NaCl solutions than in H_2O–CO_2 solutions of the same $a(H_2O)$. They interpreted this conclusion to indicate fundamental differences in solubility behaviour and silica speciation between the two solvents.

Against this interpretation, however, we note that the *actual* solubilities of quartz in H_2O–NaCl and H_2O–CO_2 fluids, expressed in terms of $X(H_2O)$, are very similar (Fig. 2), despite the different fluid structures and water activity models in the two fluids. Plots of log $X(SiO_2)$ vs. log $a(H_2O)$ (Fig. 7a) yield very different results for the two fluids, which might conventionally imply the formation of additional silica complexes involving salt components. However, we consider that this is unlikely

to be a real effect for two reasons: (1) the actual proportions of silica to water in solution are nearly the same for any $X(H_2O)$ for both H_2O–CO_2 and H_2O–NaCl fluids (Fig. 2); and (2) the apparent enhancement of quartz solubility in brine should then not occur for all $X(H_2O)$, but only at high salinities. Instead, we suggest that it may be incorrect to treat $\gamma SiO_2(aq)$ in these solutions as being equal to 1 (see also Xie and Walther 1993; Walther 1997), and thus to incorporate all non-ideality in these solutions into the $\gamma(H_2O)$ term.

The problem of the solubility of non-electrolytes in aqueous salt solutions at low temperatures and pressures is the subject of an extensive literature, but this has not generally been considered relevant to high temperature hydrothermal fluids because of the lower degree of dissociation of salts in low density, high-T water. The combination of very high pressures and temperatures in the present study means that salts are strongly dissociated, as indicated by the non-ideality of the H_2O–NaCl fluid (Aranovich and Newton 1996; Shmulovich and Graham 1996). As a result we should expect the salt to have a significant effect on the activity coefficients for the dissolved silica species, which appear to be effectively undissociated (Hershey and Millero 1986; Zotov and Keppler 2000).

The activity coefficient for a non-electrolyte species in a salt solution arises from both self-interactions, which may be negligible except at high concentration, and from interactions with salt ions. The latter interactions are significant and lead to 'salting-in' and 'salting-out' effects (Long and McDevit 1952). In the absence of further information, we have assumed that the interactions between salt ions and water molecules that are part of a hydrated aqueous silica complex will be similar to interactions between salt ions and free water molecules in the fluid. Defining $\gamma(H_2O)$ as the activity coefficient resulting from interactions between a single water molecule and salt ions in the fluid, we can expand Eq. (3) to give:

$$\log K_n = \log X(SiO_2) + n.\log \gamma(H_2O) - n.\log X(H_2O) - n.\log \gamma(H_2O) \tag{4}$$

Fig. 7 Comparative plots of **a** log $X(SiO_2)$ vs. log $a(H_2O)$ and **b** log $X(SiO_2)$ vs. log $X(H_2O)$ [Eqs. (3) and (4); see text for discussion] for quartz dissolution H_2O–NaCl and H_2O–CO_2 fluids at 0.9 GPa, 800 °C. *Solid lines* fit solubility data. *Dashed lines* are theoretical lines for $SiO_2 \cdot nH_2O$ for values of $n = 2$, 4 and 8. *Solid circles* H_2O–NaCl; *open circles* H_2O–CO_2
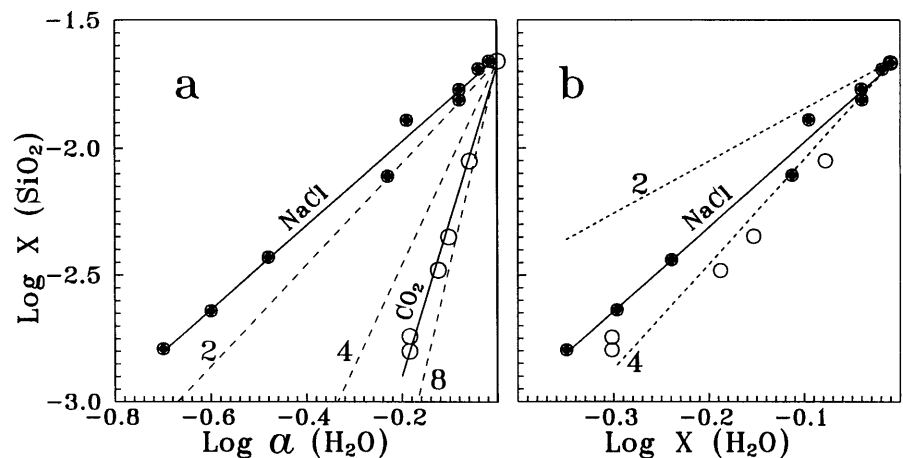
It follows from our assumption that all water–salt interactions are similar, that irrespective of the hydration number n for aqueous silica, a simple plot of log $X(SiO_{2(aq)})$ vs. log $X(H_2O)$ should yield a similar data array to that determined for the H_2O–CO_2 fluids if our assumption that silica speciation in both solvents is the same. With the exception of the apparent curvature in Fig. 6 at low $X(H_2O)$ in H_2O–CO_2 fluids, there is a striking similarity in the log $X(SiO_{2(aq)})$ vs. log $X(H_2O)$ plots for both H_2O–CO_2 and H_2O–$NaCl$ fluids (Fig. 7b). Small residual differences may reflect the untested uncertainties in our assumptions and/or the possibility of small amounts of additional Na–silica complexes being present in the H_2O–$NaCl$ fluids. We conclude that the speciation of silica in both H_2O–CO_2 and H_2O–$NaCl$ fluids at 0.9 GPa and 800 °C is comparable, is dominated by $Si(OH)_4 \cdot 2H_2O$ and/or tetrahedral hydrated species with lower hydration numbers, and is also comparable with those proposed for lower P–T conditions (Walther and Orville 1983).

Finally, quartz solubility in NaCl-rich brines does not change with pressure at the P–T conditions of our experiments, whereas solubility at low $X(NaCl)$ at 0.9 GPa is approximately double the value at 0.5 GPa (Fig. 2). This contrast implies that the structure and speciation of H_2O–$NaCl$ solutions changes in a major way between dilute solutions, which are highly dissociated at high pressures, and hydrosaline melts whose structure is not known but may be more strongly associated and less compressible. Such a contrast calls into question the application of any one simple thermodynamic model to describe quantitatively the solution behaviour of quartz and speciation of SiO_2 over a wide range of P–T–$X(NaCl)$ conditions. This is in contrast to the apparently simpler solution behaviour of quartz in H_2O–CO_2 fluids over comparably wide P–T–$X(CO_2)$ conditions. Therefore available models of silica speciation and quartz solubility in H_2O–CO_2 and H_2O–$NaCl$ fluids at high P and T, such as those proposed above, must be used with caution in application over wide ranging P–T–X(fluid) conditions, and require independent validation by in-situ spectroscopic measurement.

Discussion

By demonstrating that mineral solubility is measurable even at low water concentrations [$X(H_2O) < 0.5$] our experiments show that H_2O–CO_2 and H_2O–$NaCl$ fluids with a low water concentration may be effective transport agents and media for crystal growth in the deep crust. An important result of this study is the demonstration that levels of silica, and probably also alumina, are very much greater in lower crustal aqueous fluids than at shallow levels. Compared with the mid to upper crust, migration of comparable volumes of fluid will be marked to a greater extent by the dissolution or growth of silicate minerals, in addition to ion exchange effects. Reduced quantities of fluid and more limited permeability in the lower crust mean that metasomatic processes will not necessarily be widespread there, but where focused fluid flow has taken place, they may be qualitatively different from that which occurs at shallower levels.

There is widespread evidence for the development of high salinity fluids in the lower crust, as a result of dissolution of water into melts or, in some settings, incorporation of water into minerals through hydration reactions. The concentrations of many metals in solution are dictated by chloride content. Where sufficient quantities of salt and CO_2 are available, immiscible CO_2-rich and salt-rich fluids can coexist (Shmulovich et al. 1995; Shmulovich and Graham 1999). The comparable solubilities of quartz and speciation of SiO_2 in both H_2O–CO_2 and H_2O–$NaCl$ fluids expressed in terms of $X(H_2O)$ identified in this study indicate that the brine phase will be more effective at transporting silica than the coexisting CO_2-rich phase only to the extent that the $X(H_2O)$ of the brine is much higher than that of the CO_2-rich phase (Shmulovich and Graham 1999). We predict that other hydrated complexes show similar patterns of enrichment in brine relative to CO_2-dominated fluids, resulting in a clear association of the main rock-forming elements with metals complexed by chloride. In contrast, elements that are complexed by sulphide or other ligands that partition into a non-polar fluid may be transported predominantly in an immiscible CO_2-rich fluid.

The concentration dependence of quartz and albite solubility in H_2O–$NaCl$ and H_2O–CO_2 fluids (Fig. 1) shows a solubility decrease of at least one order of magnitude as $X(H_2O)$ decreases from 1 to 0.5, whereas diopside solubility increases by half an order of magnitude over the same range of $X(H_2O)$. Although these results may not be quantitatively applied to polyphase mineral assemblages, they emphasise the important effect that changes in fluid salinity and fluid immiscibility may have on mineral solubility and thus on fluid chemistry in the deep crust.

References

Anderson GM, Burnham CW (1965) The solubility of quartz in supercritical water. Am J Sci 263:494–511

Anderson GM, Burnham CW (1967) Reactions of quartz and corundum with aqueous chloride and hydroxide solutions at high temperatures and pressures. Am J Sci 265:12–27

Anderson GM, Burnham CW (1983) Feldspar solubility and the transport of aluminum under metamorphic conditions. Am J Sci 283-A:283–297

Aranovich LY, Newton RC (1996) H_2O activity in concentrated NaCl solutions at high pressures and temperatures measured by the brucite–periclase equilibrium. Contrib Mineral Petrol 125:200–212

Aranovich LY, Newton RC (1997) H_2O activity in concentrated KCl solutions at high pressures and temperatures measured by the brucite–periclase equilibrium. Contrib Mineral Petrol 127:261–271

Aranovich LY, Newton RC (1999) Experimental determination of CO_2–H_2O activity-composition relations at 600–1000 °C and 6–14 kbar by reversed decarbonation and dehydration reactions. Am Mineral 84:1319–1332

Budanov SV, Shmulovich KI (2000) Experimental measurement of diopside solubility in H_2O–NaCl fluids at 650 °C and 2–7.5 kbar. Geochim Int 30(2):237

Bureau H, Keppler H (1999) Complete miscibility between silicate melts and hydrous fluids in the upper mantle: experimental evidence and geochemical implications. Earth Planet Sci Lett 165:187–196

Chen CTA, Marshall WL (1982) Amorphous silica solubilities IV. Behavior in pure water and aqueous sodium chloride, sodium sulfate, magnesium chloride and magnesium sulfate solutions up to 350 °C. Geochim Cosmochim Acta 46:279–287

Crerar DA, Anderson GM (1971) Solubility and solvation reactions of quartz in dilute hydrothermal solutions. Chem Geol 8:107–122

Currie KL (1968) On the solubility of albite in supercritical water in the range 400 to 600 °C and 750 to 3,500 bars. Am J Sci 266:321–341

Davis NF (1972) Experimental studies in the system sodium–aluminatrisilicate–water: part 1: the apparent solubility of albite in supercritical water. PhD Thesis, Pennsylvania State Univ, University Park

Ford CE (1972) Furnace design, temperature distribution, calibration and seal design in internally heated pressure vessels. Prog Exp Petrol, Natural Environment Research Council, UK, Publ D2, pp 89–96

Frantz J, Marshall W (1982) Electrical conductances and ionization constants of calcium chloride and magnesium chloride in aqueous solutions at temperatures to 600 °C and pressures to 4,000 bars. Am J Sci 282:1666–1693

Goldsmith JR, Jenkins DM (1985) The hydrothermal melting of low and high albite. Am Mineral 70:924–933

Helgeson HC, Kirkham D (1974) Theoretical prediction of the thermodynamic behaviour of aqueous electrolytes at high pressures and temperatures: I. Summary of the thermodynamic/electrostatic properties of the solvent. Am J Sci 274:1089–1198

Hershey JP, Millero FJ (1986) The dependence of the acidity constants of silicic acid on NaCl concentration using Pitzer's equations. Mar Chem 18:101–105

Kerrick DM, Jacobs GK (1981) A modified Redlich–Kwong equation for H_2O, CO_2 and H_2O–CO_2 mixtures at elevated pressures and temperatures. Am J Sci 281:735–767

Lamb W, Valley JW (1988) Granulite facies amphibole and biotite equilibria, and calculated peak-metamorphic water activities. Contrib Mineral Petrol 100:349–360

Long FA, McDevit WF (1952) Activity coefficients of nonelectrolyte solutes in aqueous salt solution. Chem Rev 51:119–169

Manning CE (1994) The solubility of quartz in H_2O in the lower crust and upper mantle. Geochim Cosmochim Acta 58:4831–4839

Markl G, Bucher K (1998) Composition of fluids in the lower crust inferred from metamorphic salt in lower crust. Nature 391:781–783

Marshall WL, Chen CTA (1982) Amorphous silica solubilities V. Predictions of solubility behavior in aqueous mixed electrolyte solutions to 300 °C. Geochim Cosmochim Acta 46:289–291

Marshall WL, Franck EU (1981) Ion product of water substance, 0–1,000 °C, 1–10,000 bars: new international formulation and its background. J Phys Chem Ref Data 10:295–304

Newton RC, Manning CE (2000) Quartz solubility in H_2O–NaCl and H_2O–CO_2 solutions at deep crust–upper mantle pressures and temperatures: 2–15 kbar and 500–900 °C. Geochim Cosmochim Acta 64:2993–3005

Novgorodov PG (1975) Quartz solubility in H_2O–CO_2 mixtures at 700 °C and pressures of 3 and 5 kbar. Geokhimika 10:1484–1489

Oelkers EH, Helgeson HC (1990) Triple-ion anions and polynuclear complexing in supercritical electrolyte solutions. Geochim Cosmochim Acta 54:727–738

Paillat O, Elphick SC, Brown WL (1992) The solubility of water in $NaAlSi_3O_8$ melts: a re-examination of Ab–H_2O phase relations and critical behaviour at high pressures. Contrib Mineral Petrol 112:490–500

Plyusnina LP, Likhoidov GG, Nekrasov IY, Scheka JA (1997) Pt solubility in water–chloride media in presence of Mn oxides at 300–500 °C, 1 kbar. Dokl Acad Sci 353:631–633

Quist AS, Marshall WL (1968) Electrical conductances of aqueous sodium chloride solutions from 0 to 800 °C and pressures to 4,000 bars. J Phys Chem 72:684–703

Ryabchikov ID, Schreyer W, Abraham K (1982) Compositions of aqueous fluids in equilibrium with pyroxenes and olivines at mantle pressures and temperatures. Contrib Mineral Petrol 79:80–84

Shen AH, Keppler H (1997) Direct observation of complete miscibility in the albite–H_2O system. Nature 385:710–712

Shettel DL (1974) The solubility of quartz in supercritical H_2O–CO_2 fluids. MSc Thesis, Pennsylvania State University, University Park

Shmulovich KI, Graham CM (1996) Melting of albite and dehydration of brucite in H_2O–NaCl fluids to 9 kbars and 700–900 °C: implications for partial melting and water activities during high pressure metamorphism. Contrib Mineral Petrol 124:370–382

Shmulovich KI, Graham CM (1999) An experimental study of phase equilibria in the system H_2O–CO_2-NaCl at 800 °C and 9 kbar. Contrib Mineral Petrol 136:247–257

Shmulovich KI, Shmonov VM, Zharikov VA (1982) The thermodynamics of supercritical fluid systems. Advances in physical geochemistry, vol 2. Springer, Berlin Heidelberg New York, pp 173–190

Shmulovich KI, Tkachenko SI, Plyasunova NV (1995) Phase equilibria in fluid systems at high pressures and temperatures. In: Shmulovich KI, Yardley BWD, Gonchar G (eds) Fluid in the crust. Chapman and Hall, London, pp 193–214

Skippen G, Trommsdorff V (1986) The influence of NaCl and KCl on phase relations in metamorphosed carbonate rocks. Am J Sci 286:81–104

Sommerfeld RA (1967) Quartz solution reaction:400–500 °C, 1,000 bars. J Geophys Res 72:4253–5257

Stalder R, Ulmer P, Thompson AB, Gunter D (2000) Experimental approach to constrain second critical endpoints in fluid/silicate systems: near-solidus fluids and melts in the system albite–H_2O. Am Mineral 85:68–77

Touret J (1985) Fluid regime in southern Norway: a record of fluid inclusions. In: Tobi AC, Touret JLR (eds) The deep Proterozoic crust in the north Atlantic provinces. NATO ASI Series C158. Reidel, Dordrecht, pp 517–549

Touret JLR (1995) Brines in granulites: the other fluid. Bol Soc Esp Mineral 18(1):250–251

Walther JV (1986) Mineral solubilities in supercritical H_2O solutions. Pure Appl Chem 58:1585–1598

Walther JV (1991) Determining the thermodynamic properties of solutes in crustal fluids. Am J Sci 291:453–472

Walther JV (1997) Determination of activity coefficients of neutral species in supercritical H_2O solutions. Geochim Cosmochim Acta 61:3311–3318

Walther JV, Helgeson HC (1977) Calculation of the thermodynamic properties of aqueous silica and the solubility of quartz and its polymorphs at high pressures and temperatures. Am J Sci 277:1315–1351

Walther JV, Helgeson HC (1980) Description and interpretation of metasomatic phase relations at high pressures and temperatures: I. Equilibrium activities of ionic species in non-ideal mixtures of CO_2 and H_2O. Am J Sci 280:576–606

Walther JV, Orville PM (1983) The extraction–quench technique for determination of the thermodynamic properties of solute complexes: application to quartz solubility in fluid mixtures. Am Mineral 68:731–741

Webster JD (1992a) Fluid–melt interactions involving Cl-rich granites: experimental study from 2 to 8 kbar. Geochim Cosmochim Acta 56:659–678

Webster JD (1992b) Water solubility and chlorine partitioning in Cl-rich granitic systems: effects of melt composition at 2 kbar and 800 °C. Geochim Cosmochim Acta 56:679–687

Woodland AB, Walther JV (1987) Experimental determination of the solubility of the assemblage paragonite, albite, and quartz in supercritical H_2O. Geochim Cosmochim Acta 51:365–372

Xie Z, Walther JV (1993) Quartz solubilities in NaCl solutions with and without wollastonite at elevated temperatures and pressures. Geochim Cosmochim Acta 57:1947–1955

Yardley BWD (1996) The evolution of fluids through the metamorphic cycle. In: Jamtveit B, Yardley, BWD (eds) Fluid flow and transport in permeable rocks. Chapman and Hall, London, pp 99–119

Yardley BWD, Bottrell SH (1988) Immiscible fluids in metamorphism: implications of two-phase flow for reaction history. Geology 16:199–202

Zotov N, Keppler H (1999) In-situ Raman spectra of dissolved silica species in aqueous fluids to 900 °C and 14 kbar. Am Mineral 85:600–603